

## Supporting Information

### **Regulating Crystallinity to Balance the Electrochemical Performance of Cobalt-tin oxide**

#### **Composite Anode for Sodium-Ion Batteries**

*Ying Yang,<sup>1,2\*</sup> Ruirui Zhao,<sup>2</sup> Chaofeng Liu,<sup>2</sup> Yaping Qi,<sup>1,4</sup> Dan Hu,<sup>1</sup> Duanhui Si,<sup>3</sup> Yong P. Chen<sup>1,4,5,6\*</sup>*

1 Department of Engineering Science, Faculty of Innovation Engineering, Macau University of Science and Technology, Av. Wai Long, Macao SAR, 999078, China

2 Institute of New Energy for Vehicles, School of Materials Science and Engineering, Tongji University, Shanghai, 201804, China

3 State Key Laboratory of Structural Chemistry, Fujian Institute of Research on the Structure of Matter, Chinese Academy of Sciences, Fuzhou 350002, China

4 Advanced Institute for Materials Research (WPI-AIMR), Tohoku University, Sendai 980-8577, Japan

5 Department of Physics and Astronomy and Elmore Family School of Electrical and Computer Engineering and Birck Nanotechnology Center and Purdue Quantum Science and Engineering Institute, Purdue University, West Lafayette, IN 47907, USA

6 Institute of Physics and Astronomy and Villum Center for Hybrid, Quantum Materials and Devices Aarhus University, Aarhus-C 8000, Denmark

\*Corresponding authors: [yangying632882@126.com](mailto:yangying632882@126.com); [yochen@must.edu.mo](mailto:yochen@must.edu.mo)

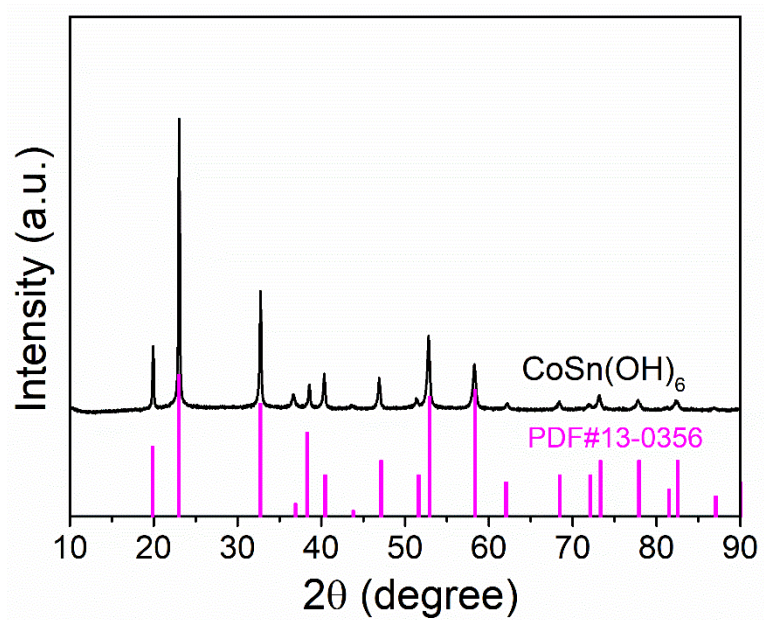


**Figure S1.** The XRD pattern of the precursor.

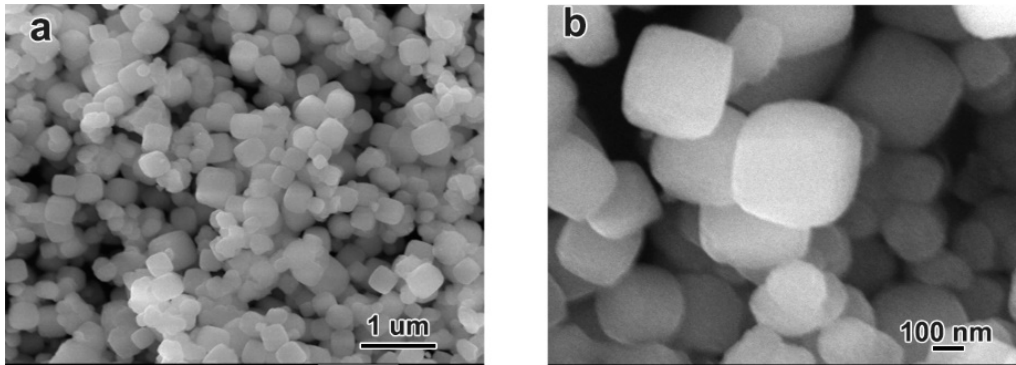


**Figure S2.** The SEM images of the precursor  $\text{CoSn}(\text{OH})_6$  at different resolutions.

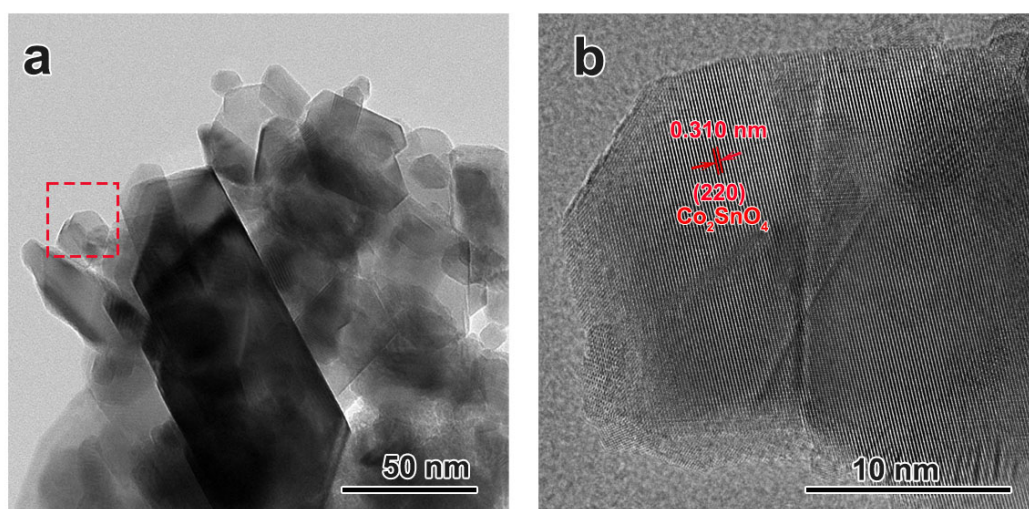


**Figure S3.** The high resolution TEM images of CSO-C at two different resolutions (See scale bars).

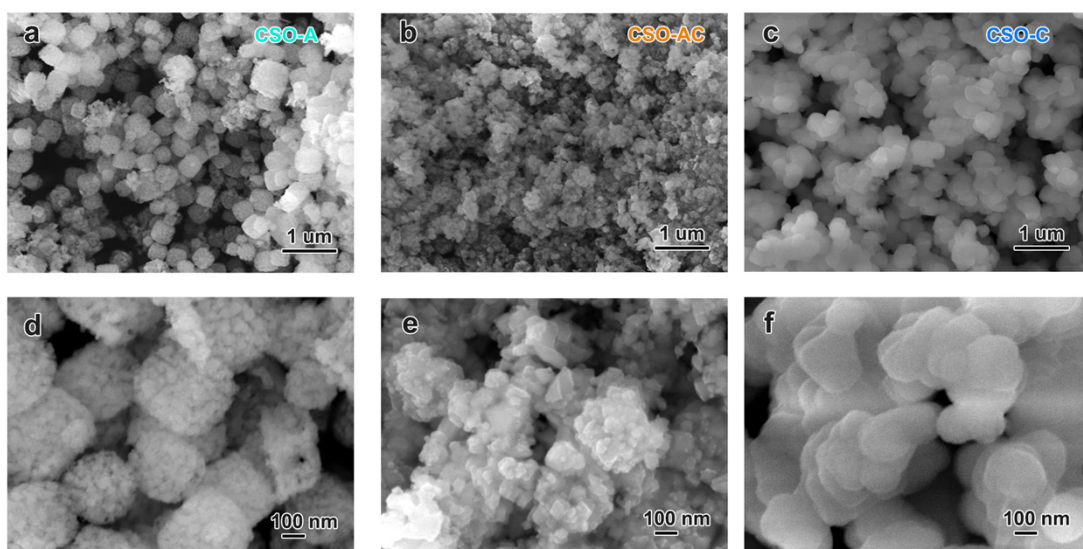


**Figure S4.** The SEM images of (a, d) CSO-A, (b, e) CSO-AC, (c, f) CSO-C at two different resolutions (See scale bars).

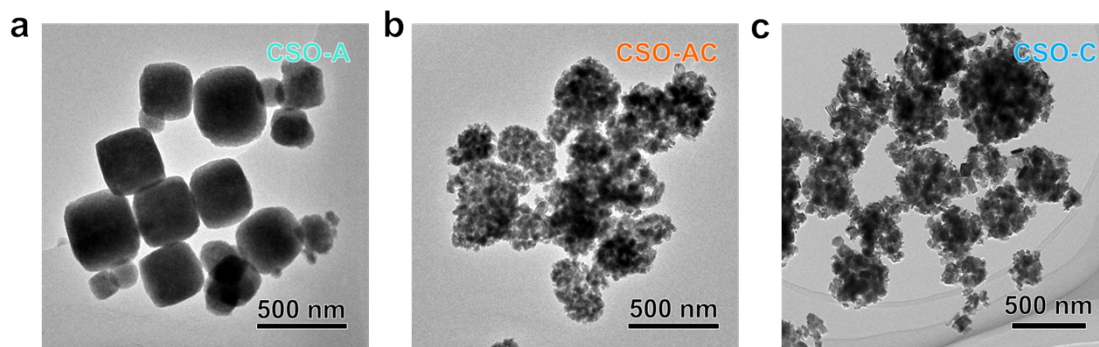


**Figure S5.** The TEM images of (a) CSO-A, (b) CSO-AC, (c) CSO-C at the same resolution (See scale bars).

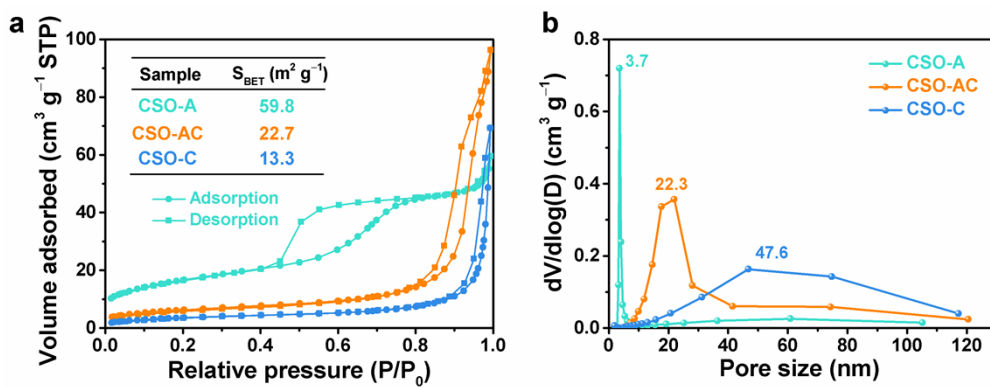


**Figure S6.** (a) Nitrogen adsorption (data in filled circles) and desorption (data in squares) isotherms, (b) BJH pore size distributions of CSO-A, and CSO-C.



**Figure S7.** The electronic photographs of CSO-C.

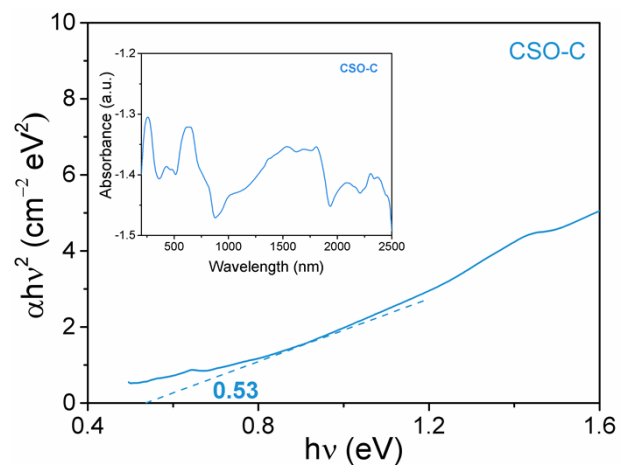


**Figure S8.** The plots of  $(\alpha h\nu)^2$  and  $h\nu$ ; the inset shows the UV-vis DRS absorption spectra.

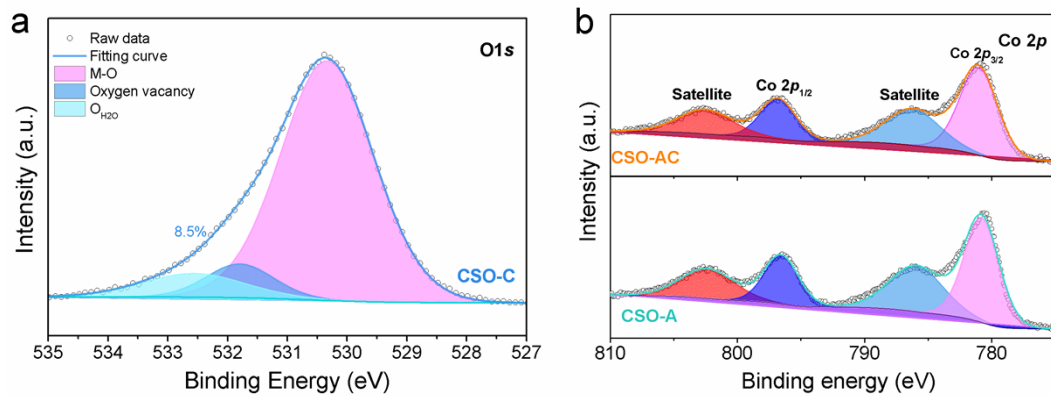


**Figure S9.** (a) The high-resolution O 1s XPS spectra of CSO-C. (b) The high-resolution Co 2p XPS spectra of CSO-A and CSO-AC samples.

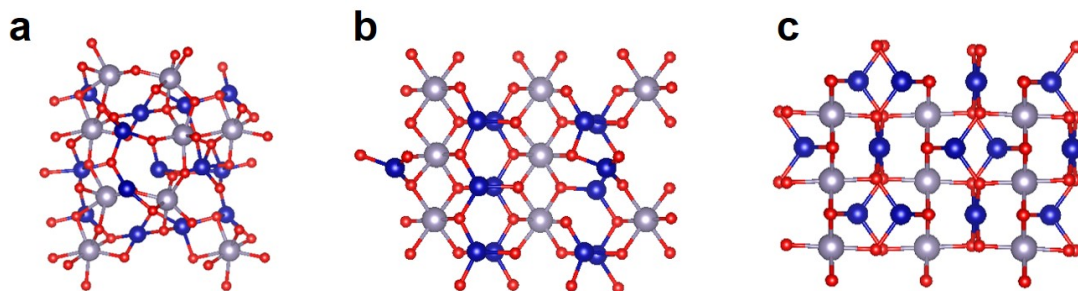


**Figure S10.** The calculated structure models of tin-cobalt oxide (CSO) with different degrees of crystallinity. (a) CSO-A with amorphous structure; (b) CSO-AC with amorphous and crystal structure; (c) CSO-C with high crystalline structure.

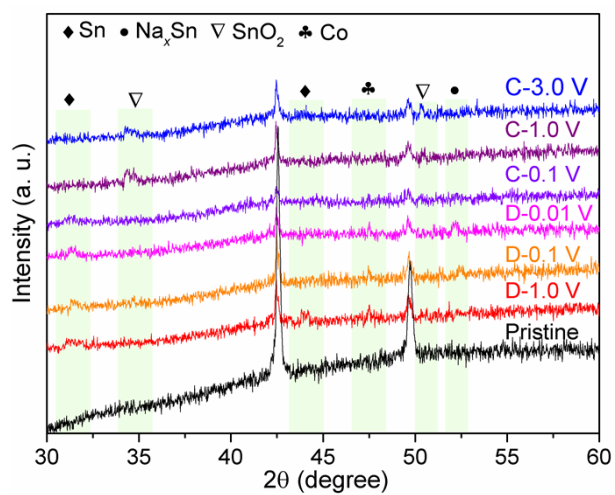


**Figure S11.** Ex situ XRD patterns of CSO-A electrode collected at various charge/discharge states in  $\text{Na}^+$  half cells.

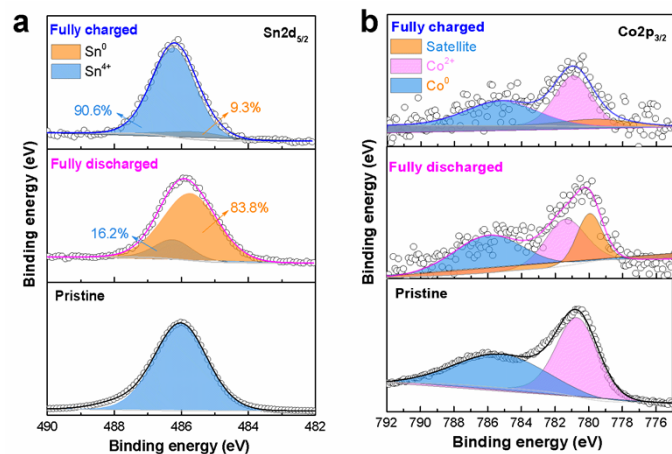


**Figure S12.** Ex situ XPS spectra of (a) Sn 3d<sub>5/2</sub> and (b) Co 2p<sub>3/2</sub> in CSO-A at the pristine, fully discharged, and fully charged states.

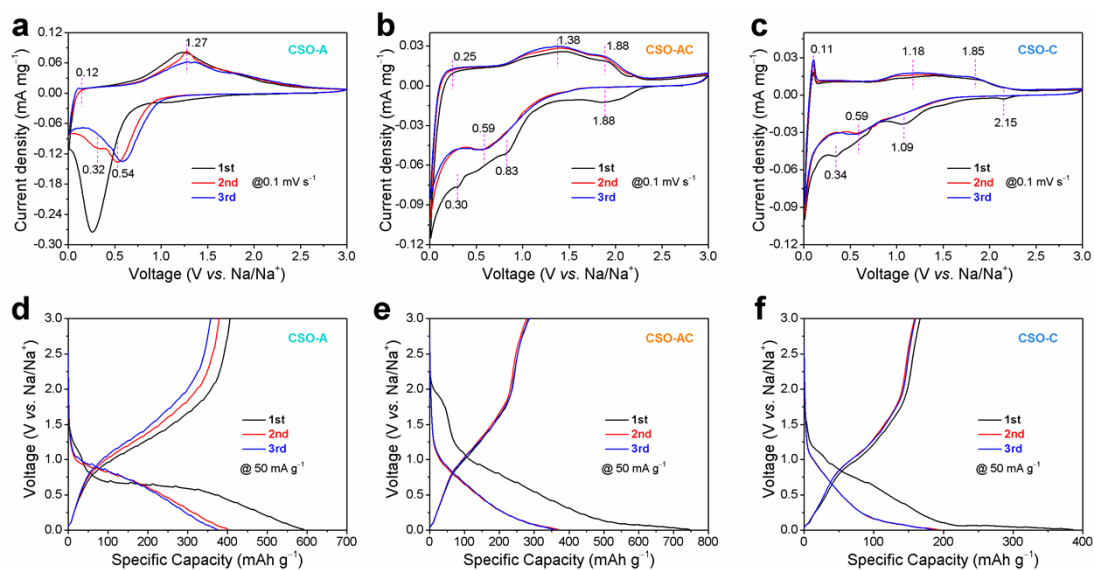


**Figure S13.** The cyclic voltammetry curves of the as-synthesized (a) CSO-A, (b) CSO-AC, and (c) CSO-C electrode at a scan rate of  $0.1 \text{ mV s}^{-1}$  in a voltage window of  $0.01 \sim 3 \text{ V vs. Na/Na}^+$  for the first three cycles. The charge-discharge profiles of the as-synthesized (d) CSO-A, (e) CSO-AC, and (f) CSO-C electrode at a current density of  $50 \text{ mA g}^{-1}$  in a voltage window of  $0.01 \sim 3 \text{ V vs. Na/Na}^+$  for the first three cycles.

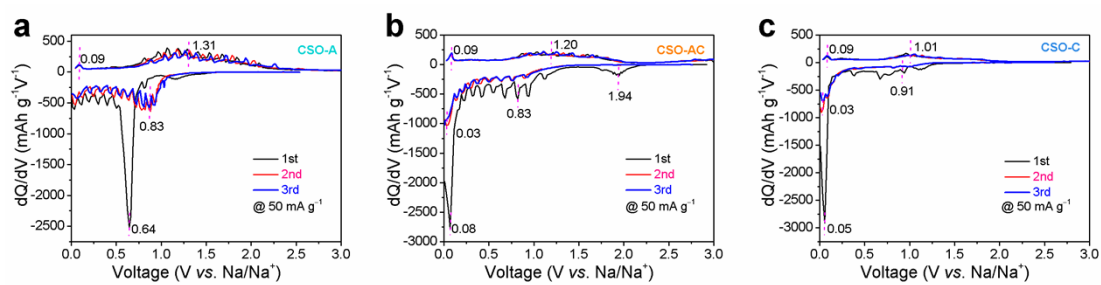


**Figure S14.** Differential capacity plots ( $dQ/dV$ ) of the (a) CSO-A, (b) CSO-AC, and (c) CSO-C electrode at a current density of  $50 \text{ mA g}^{-1}$  in the voltage range between 0.01 and 3.0 V vs.  $\text{Na/Na}^+$  for the second cycle. The  $dQ/dV$  plots were obtained from the charge/discharge profiles of CSO as shown in Figures S10d ~ S10f.

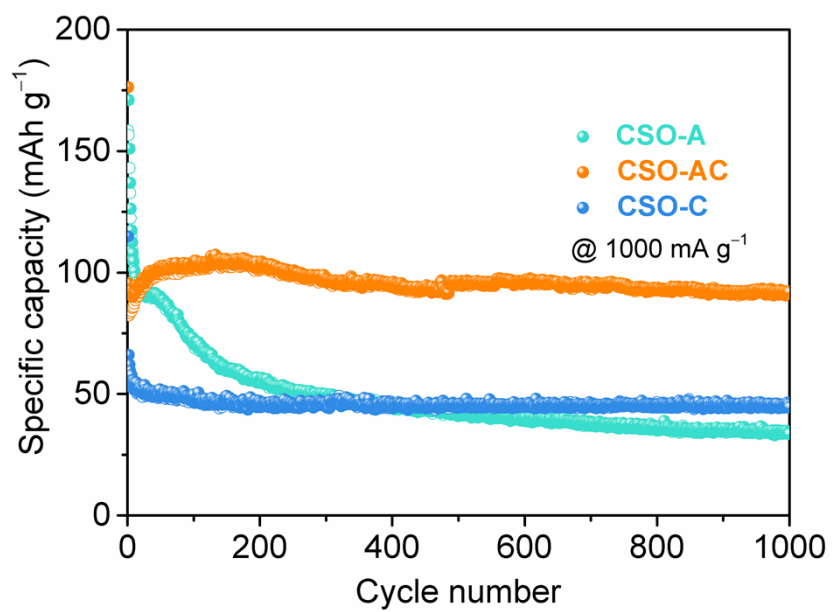


**Figure S15.** Cycle stability of the CSO-A and CSO-AC samples at a current density of 50 mA g<sup>-1</sup> for activated and 500 mA g<sup>-1</sup> for cycling.

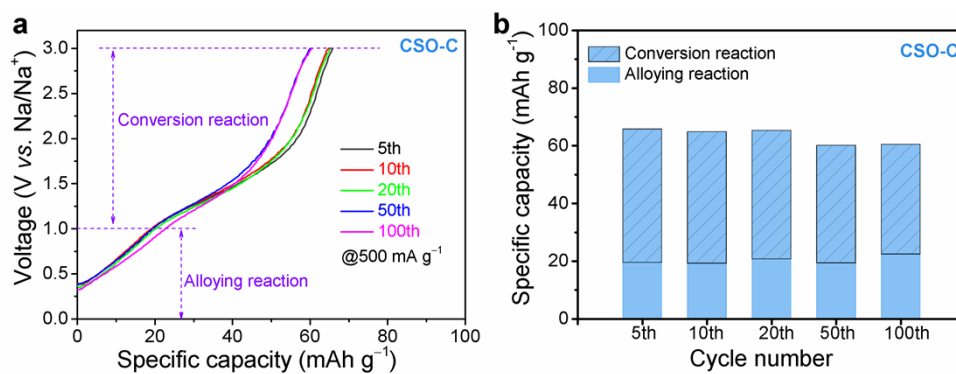


**Figure S16.** (a) The charge curves of CSO-C electrode at the 5th, 10th, 20th, 50th, and 100th cycles at a current density of 500 mA g<sup>-1</sup>. (b) The reversible specific capacity of CSO-C electrode from the conversion reaction and alloying reaction process, separately, at the 5th, 10th, 20th, 50th, and 100th cycles. The data were collected from the charge curves in Figure S12a at a current density of 500 mA g<sup>-1</sup>.

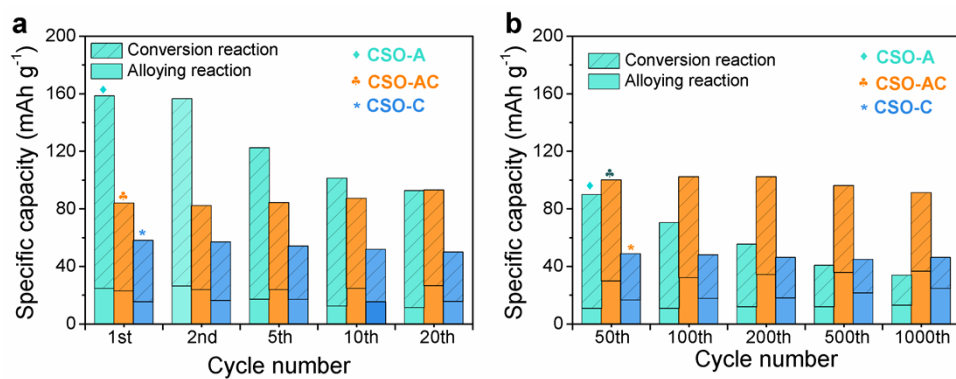


**Figure S17.** (a) The specific capacity of CSO-A, CSO-AC, and CSO-C electrodes at the 1st, 2nd, 5th, 10th, and 20th cycles from the process of the conversion reaction and alloying reaction, separately. (b) The specific capacity of CSO-A, CSO-AC, and CSO-C electrodes at the 50th, 100th, 200th, 500th, and 1000th cycles from the process of the conversion reaction and alloying reaction, separately. All the data were collected from the charge curves of CSO electrodes at a current density of 1000 mA g<sup>-1</sup>.

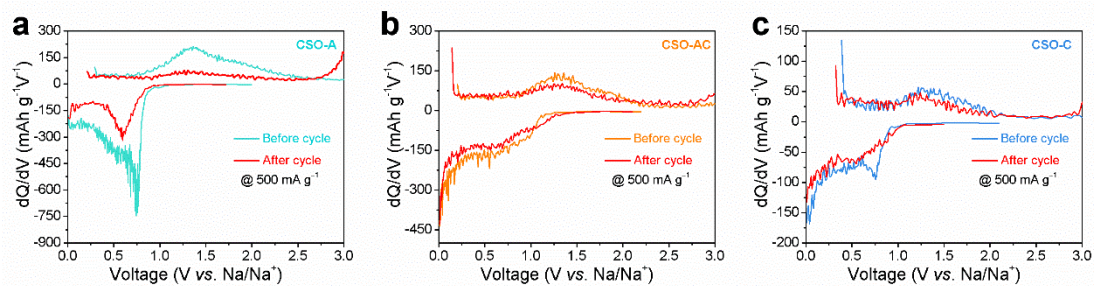


**Figure S18.** Differential capacity plots of the CSO-A, CSO-AC, and CSO-C electrodes at a current density of  $500 \text{ mA g}^{-1}$  for the charge/discharge profiles of the 5th and 100th cycles.

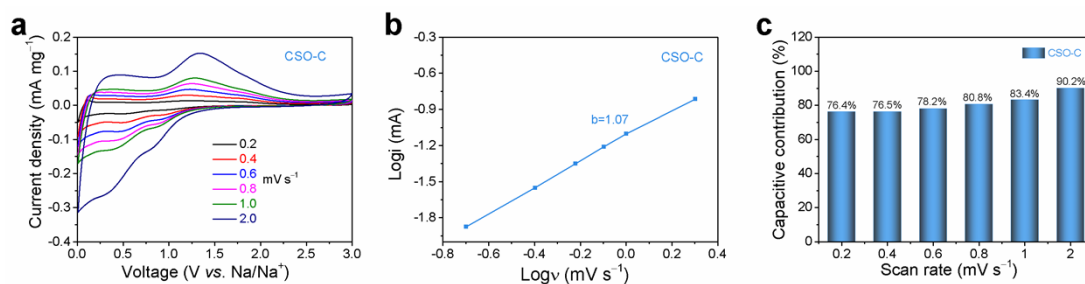


**Figure S19.** a) CV curve of CSO-C at a sweep rate from 0.2 to 2.0  $\text{mV s}^{-1}$ . b) The relationship between logarithm cathodic peak current and logarithm scan rates at a voltage of 1.50 V. c) The percentage of the capacitance contribution for CSO-C electrodes at different scan rates. the estimated capacitive current contribution is shown in the shaded region.

Table S1. The key structure and electrochemical parameters of the CSO-A and CSO-AC were collected from the results of various experimental characterization.

Sample	T/ °C	Crys	C <sub>ov</sub>	S <sub>BET</sub>	Band gap	C <sub>Initial</sub>	CR <sub>Total</sub>	CR <sub>Conversion</sub>	Pesudo
CSO-A	400	A	31.0	59.8	0.75	408	53.8%	49.3%	75.1%
CSO-AC	600	A, C	13.1	22.7	0.69	289	96.1%	89.5%	88.9%
CSO-C	800	C	8.5	13.3	0.53	168	91.9%	82.3%	90.2%

T: Annealed Temperature;

Crys: Crystallinity, A: Amorphous, C: crystal;

C<sub>ov</sub>: Content of oxygen vacancy calculated from the results of O1s XPS spectra;

S<sub>BET</sub>/ m<sup>2</sup> g<sup>-1</sup>: Specific surface area calculated based on BET method;

Band gap /eV: collected from the results of UV-vis;

C<sub>Initial</sub>/ mAh g<sup>-1</sup>: Initial reversible specific capacity from the charge curve at the current density of 50 mA g<sup>-1</sup>;

Capacity retention (CR<sub>Total</sub> retention): the percent of reversible specific capacity after and before cycle based on the results of cycling stability at a current density of 500 mA g<sup>-1</sup>;

Capacity retention of conversion reaction (CR<sub>Conversion</sub>): the percent of reversible specific capacity contributed by conversion reaction based on the results of charge curve for the fifth cycle and 100th cycle at a current density of 500 mA g<sup>-1</sup>;

Pesudo: Pseudo-capacitance contribution at a scan rate of 2.0 mV s<sup>-1</sup>.

Table S2. The key structure and electrochemical parameters of the three tin-cobalt oxide with different degrees of crystallinity. These data are collected from the results of various theoretical calculations.

Sample	Crystal	Band gap/ eV	Binding energy/ eV	Na <sup>+</sup> diffusion barriers/ eV
CSO-A	Amorphous	0.11	-3.65	0.41
CSO-L	Low crystallinity	0.06	-2.58	0.77
CSO-H	High crystallinity	0.00	-1.67	1.35